ACS OMEGA

Open Access

http://pubs.acs.org/journal/acsodf

Article

Fe_3O_4/Graphene Oxide/Chitosan Nanocomposite: A Smart Nanosorbent for Lead(II) Ion Removal from Contaminated Water

Linh Quang Vo, Anh-Tuan Vu, Thu Dieu Le, Chinh Dang Huynh, and Hoang Vinh Tran*

Cite This: *ACS Omega* 2024, 9, 17506−17517

Read Online

ACCESS | Metrics & More | Article Recommendations | Supporting Information

ABSTRACT: A new graphene oxide (GO) nanocomposite that contains chitosan, a biological polymer, combined with a magnetic nanoparticle inorganic material (Fe_3O_4) was successfully prepared and applied for the adsorption of Pb(II) from aqueous solutions. The structural and morphological properties of the GO/Fe_3O_4/CS (GFC) nanocomposites were characterized by X-ray diffraction, scanning electron microscopy, and energy-dispersive X-ray spectroscopy. Influent factors for Pb(II) adsorption, including the contacting time, pH of the working medium, working temperature, and adsorbent dosage on the adsorption efficiency, have been optimized. Under optimized conditions, the adsorption isotherm results indicated that the Langmuir model provided a better description for the adsorption of Pb(II) onto the GFC nanosorbent than the Freundlich model. The maximum adsorption capacity (q_{max}) was 63.45 mg g^{-1}. The pseudo-second-order kinetic model (R^2 = 0.999) was fitted with the experimental results, implying that the adsorption of Pb(II) onto GFC is a chemical process. The thermodynamic studies demonstrated the exothermic nature of the adsorption process. Another advantage of the GFC nanosorbent for Pb(II) removal is its capability to be easily recovered under the use of an external magnet and subsequently regenerated. Our work demonstrated that the removal efficiency was stable after several regeneration cycles (i.e., approximately 12% reduction after four successive adsorption−desorption cycles), implying that the GFC nanosorbent exhibits satisfactory regeneration performance. Therefore, with high removal efficiency, high adsorption capacity, and stable reusability, the GFC nanocomposite is a remarkable application potential adsorbent for the in situ treatment of Pb(II) ion-containing aqueous solutions.

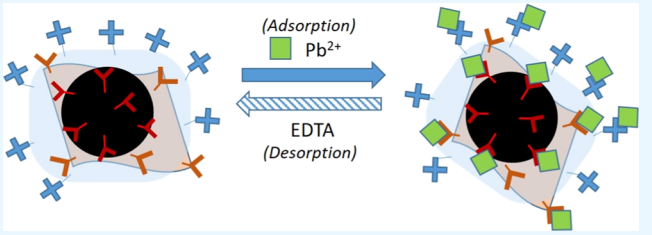

INTRODUCTION

Along with technological advancement, toxic metal contamination has become a severe problem that threatens human health.[1] Lead, mercury, chromium, arsenic, cadmium, zinc, copper, and nickel are the most common contaminants found in contaminated surface water, groundwater, and industrial wastewater.[2−6] Exposure to heavy metals imparts serious threats to the ecosphere and human health owing to their high toxicity, nonbiodegradability, and environmental persistence.[7] As a ubiquitous and priority pollutant categorized by the US Environmental Protection Agency (USEPA), Pb(II) is primarily discharged from various sources, including mining, battery and metallurgical manufacturing, printing and painting industries, and smelting operations.[8−10] The World Health Organization and the US Environmental Protection Agency have set the permissible limit of Pb(II) concentration in drinking water to be 0.01 and 0.015 mg L^{-1}.[2] If contaminated water is drunk for a long time, lead can accumulate in human organs and cause different types of diseases that affect the blood, kidney, brain, and heart.[11] Thus, the contents of Pb(II) ions in industrial effluents must be completely eliminated or minimized before they are discharged into receiving water bodies.

To date, numerous methods, including precipitation, ion exchange, reverse osmosis, electrochemical treatments, membrane separation, coagulation, flotation, and biosorption processes, have been applied for the removal of free Pb(II) ions in contaminated water;[12−21] although these techniques are reliable, they are not economical or effective. These treatment procedures have limiting factors, including their high energy and chemical requirements, incomplete removal, generation of secondary pollution, and toxic sludge.[22,23] Currently, the adsorption process is considered one of the most attractive technologies for heavy metal ion treatment in contaminated water owing to its high efficiency, low cost, easy operation, and no secondary pollution.

In recent years, graphene oxide (GO) has been considered an excellent adsorbent for the removal of heavy metal ions because it has a very high specific surface area and contains widespread functional groups that enhance the adsorption capacity (q_{max}).[6,24,25] Based on favorable adsorption properties, graphene-based adsorbents have been successfully utilized to

Received: January 15, 2024
Revised: March 18, 2024
Accepted: March 21, 2024
Published: April 3, 2024

scavenge different types of heavy metals from aqueous media.[26] However, as micro or nanosized, GO is difficult to recover after the adsorption process; therefore, GO is usually used as a part of an adsorbent composite.[2,25,27−31] One of the most suitable polymers that can be conjugated with GO is chitosan (CS). It is a natural polymer obtained through the deacetylation process of chitin and possesses rich functional groups (−NH_2 and −OH) that exhibit strong complexing ability with free heavy metal ions on its molecular backbone endow. Therefore, it is highly promising for the uptake of free heavy metal ions.[32−36] Furthermore, the protonated amino groups formed under acidic conditions could capture anionic pollutants through electrostatic attraction.[37−39] Therefore, GO and CS are two outstanding candidates in this field, considering adsorption efficiency toward heavy metal ions. Unfortunately, like GO, the GO/CS nanocomposite as micro/nanosized is also difficult to recover after the adsorption process, leading to the GO/CS nanocomposite being a nonrenewable adsorbent.

In this work, we propose a combination of GO and CS with magnetite nanoparticles (Fe_3O_4) to form a GO/Fe_3O_4/CS (GFC) nanocomposite adsorbent. This approach is an effective way to simply overcome the separation problem because of the presence of Fe_3O_4 nanoparticles in GFC, leading to the magnetic separation of the GFC adsorbent after adsorption. Finally, the recovery and regeneration of the adsorbent can be done easily. In addition, the GFC nanocomposite still consists of a large specific surface area and abundant surface groups coming from GO and CS, which can enhance the adsorption capacity. The obtained results also indicated excellent adsorption performance with an application to remove Pb(II) ions. These nanocomposite beads feature extraordinary adaptability, low cost, easy operation, and explicit regeneration, which are useful not only for the removal of Pb(II) ions but also for other heavy metal ions from contaminated water.

MATERIALS AND METHODS

Materials. Graphite flakes (>99 wt %), sulfuric acid (H_2SO_4, 98 wt %), sodium nitrate (NaNO3), potassium permanganate ($KMnO_4$), iron(II) sulfate heptahydrate ($FeSO_4{\cdot}7H_2O$, 99 wt %), iron(III) chloride hexahydrate ($FeCl_3{\cdot}6H_2O$, 99 wt %), sodium hydroxide (NaOH, 96 wt %), acetic acid (CH_3COOH, 99 wt %), CS ($(C_8H_{13}O_5N)_n$, DD% >75%), hydro peroxide (H_2O_2, 33%), 4-(2-pyridylazo)-rezoxin (PAR, $C_{11}H_8N_3NaO_2{\cdot}H_2O$, 99 wt %), lead(II) nitrate ($Pb(NO_3)_2$, 99.5 wt %), sodium acetate trihydrate ($CH_3COONa{\cdot}3H_2O$, 99 wt %), ammonia (NH_3, 25−28%), and EDTA disodium salt (Na_2EDTA, 99.4 wt %) were purchased from Sigma-Aldrich.

Preparation of GO. Using Hummers's method, GO was synthesized in our laboratory from Vietnam's graphite. Detailed conditions and experiments are described in the Supporting Information.

Synthesis of Magnetic Nanoparticles. Magnetic nanoparticles (Fe_3O_4) were synthesized by a co-precipitation method from Fe(II) and Fe(III) mixture salts. Typically, 1.078 g of $FeSO_4{\cdot}7H_2O$ and 2.098 g of $FeCl_3{\cdot}6H_2O$ were poured into 50 mL of distilled water with stirring to form a mixed solution. Next, a 2 M NaOH solution was added to the aforementioned mixture using a peristaltic pump under constant magnetic stirring, and the final pH was 11. The Fe_3O_4 magnetite nanoparticles were formed following a chemical reaction:

$$Fe^{2+} + 2Fe^{3+} + 8OH^- \rightarrow Fe_3O_4(s) + 4H_2O \quad (1)$$

The resulting particles were magnetically separated and repeatedly washed with distilled water and ethanol until they reached pH 7. Finally, the Fe_3O_4 product was redispersed into DI water to form a black suspension for use.

Preparation of GFC Nanocomposite. For a typical synthesis, 0.225 g of GO was dispersed into 22.5 mL of distilled water using ultrasonication to create a 10 mg mL^{-1} GO solution. Subsequently, 1.05 g of the as-prepared Fe_3O_4 slurry was continuously added, followed by the addition of 22.5 mL of 10 mg mL^{-1} CS solution (5.0 g of CS into 10 mL of acetic acid (1%. v/v)) to form a mixture. The mixture was sonicated for 30 min at room temperature to obtain a homogeneous slurry. Then, the 1 M NaOH solution was added to the aforementioned mixture under constant magnetic stirring until the pH reached 8. The final bulk black precipitate was magnetically collected, rinsed with DW until it reached a neutral pH of 7, and then dried in an oven at 80 °C for 24 h to obtain a GFC (15:70:15) nanocomposite. The synthesis procedure is shown in Figure S1. To investigate the effect of the mass ratio of each component in the GFC composite on Pb(II) adsorption efficiency, the mass ratios of GO, Fe_3O_4, and CS were taken as 15:60:25, 10:70:20, 15:70:15, and 10:80:10, respectively.

Adsorption Experiment. The adsorption of Pb(II) on the GCE nanosorbent was performed at room temperature by adding 0.05 g of GFC to a beaker containing 100 mL of a specific concentration of $Pb(NO_3)_2$. The mixture was ultrasonicated for 10 min at RT. After a particular time, 2 mL of the solution was taken to determine the residue concentration of Pb(II) by spectrophotometric assay using the following protocol: 1 mL of the sample solution was mixed with 4-(2-pyridylazo) rezocxin (PAR), sodium acetate, and NH_3 at pH of 10. After the formation of the Pb(II)-4-(2-pyridylazo) rezocxin complex, the concentration of Pb(II) ions was determined from the absorbance peak at 520 nm on a UV−vis spectrophotometer and a calibration curve (Figure S2). The equilibrium adsorption capacity (q_e) and the removal efficiency (R_e) of the dye are determined by eqs 2 and 3, respectively.

$$q_e = \frac{(C_o - C_e) \times V}{m} \quad (2)$$

$$R_e = \frac{C_o - C_t}{C_o} \times 100\% \quad (3)$$

where q_e (mg g^{-1}) is the equilibrium adsorption amount; C_o (mg L^{-1}), C_e (mg L^{-1}), and C_t are the initial, equilibrium, and concentrations at t time, respectively; V (L) is the solution volume; and m (g) is the mass of the adsorbent.

Material Characterizations. The XRD pattern was analyzed by a Bruker D8 Advance diffractometer (Germany) with Cu Kα irradiation (40 kV, 40 mA) to investigate the crystalline phase of the samples. The 2θ ranging from 5 to 80° was selected to analyze the crystal structure. The chemical composition of the samples was determined by a JEOL scanning electron microscope and a JSM-5410 energy-dispersive X-ray (SEM/EDS) spectrometer. The magnetization measurement of the Fe_3O_4 and GFC nanocomposite samples was conducted using a vibrating sample magnetometer (VSM, PPMS 6000) at RT with an applied magnetic field of 70 kOe and sensitivity of 5 × 10^{-6} emu. The pH_{PZC} for GFC was determined by a pH meter with a volume of 100 mL of 0.02 M

https://doi.org/10.1021/acsomega.4c00486
ACS Omega 2024, 9, 17506−17517

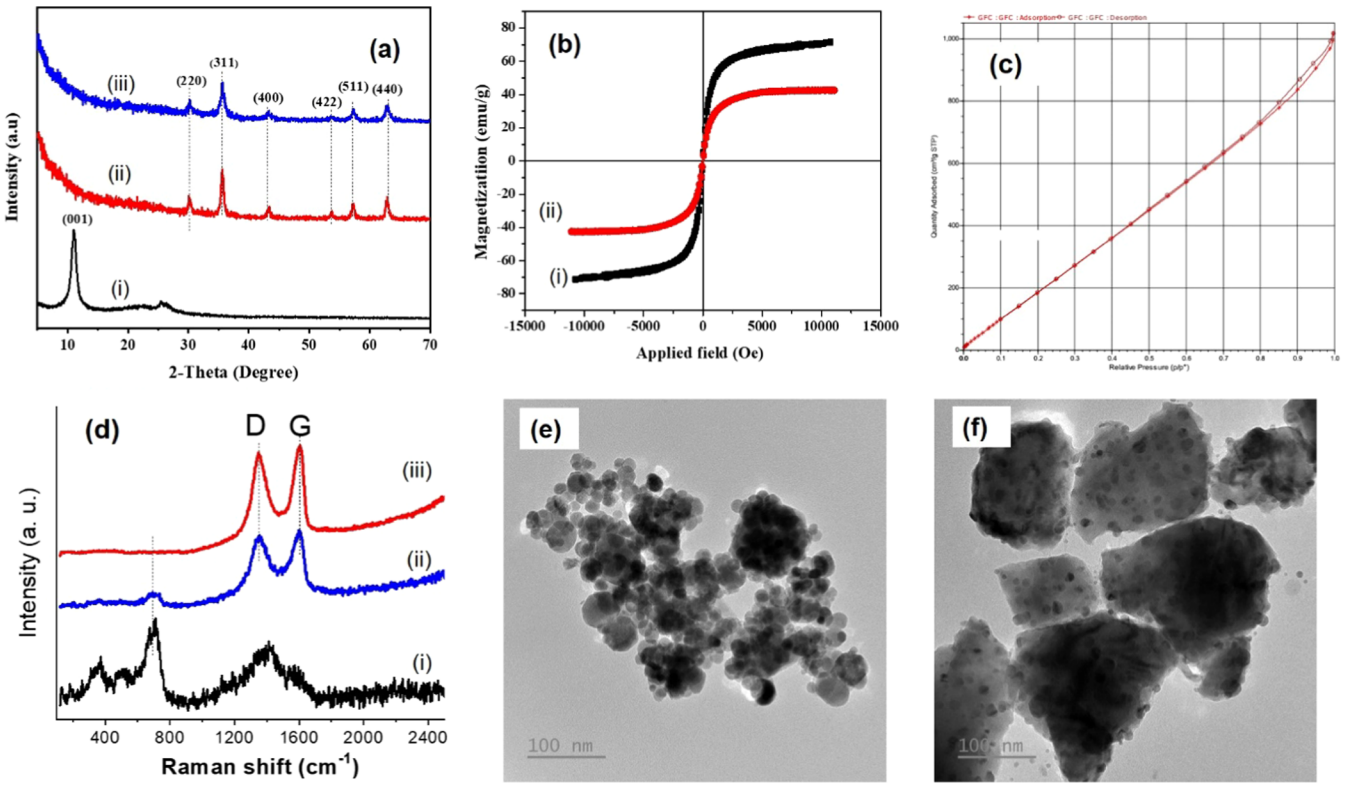

Figure 1. (a) XRD patterns of (i) GO, (ii) Fe_3O_4 nanoparticles, and (iii) GFC nanocomposite. (b) VSM of (i) Fe_3O_4 nanoparticles and (ii) GFC nanocomposite. (c) Nitrogen (N_2) adsorption−desorption isotherm and (d) Raman spectra of (i) Fe_3O_4 nanoparticles, (ii) GFC, and (iii) GO. (e, f) TEM images of (e) Fe_3O_4 nanoparticle and (f) GFC.

KNO_3 salt at different pH values (control by using NaOH 1 M or HCl 1 M) before and after adding 0.05 g of GFC and stirring for 24 h at RT. Finally, the initial (pH_i) vs final (pH_f) values curve was depicted to estimate the pH_{PZC} value.

RESULTS AND DISCUSSION

Physicochemical Characterization of GFC Nanocomposites. Figure 1a shows the XRD patterns of pure GO (curve (i)), Fe_3O_4 (curve (ii)), and the GO/Fe_3O_4/CS (GFC) nanocomposite (curve (iii)). The characteristic peak at 11.9° in the XRD of GO (cure (i)) can be assigned to the interlayered stacking pattern (001). This result is in agreement with the claims of GO.[40] The XRD spectra of Fe_3O_4 (curve (ii)) and GFC nanocomposite (curve (iii)) show that the synthesized Fe_3O_4 material is a single phase with a low diffraction baseline, indicating a complete crystalline phase. The characteristic peaks of Fe_3O_4 are presented at 2θ = 30.21, 37.13, 43.37, 53.81, 57.05, and 63.44°, corresponding to (220), (222), (400), (422), (511), and (440) (JCPDS file, PDF No. 65−3107),[1] thereby confirming the formation of the magnetic spinel nanocrystal phase of Fe_3O_4 in accordance with the standard. Compared with the bare Fe_3O_4 sample, the diffraction curve of the characteristic peaks of Fe_3O_4 in the GFC composites is weaker, indicating that the Fe_3O_4 particles have been coated with amorphous CS and GO. For the GFC composite, the characteristic peak at 2θ = 11.9° indicates that the presence of GO did not clearly appear, which can be attributed to the low GO content in this sample and also caused by coating CS and Fe_3O_4 onto the GO layers.[41] Furthermore, the XRD pattern of the GFC composite (curve (iii)) reveals that no impurity phases can be observed, implying the high purity of the GFC composite. Line broadening in the pattern can be evaluated quantitatively using the Debye−Scherer equation (eq 4), which presents a relationship between peak broadening in XRD and particle size:

$$d = k\cdot\lambda/\beta\cdot\cos(\theta) \quad (4)$$

where d (nm) is the domain size of the Fe_3O_4 crystal, k is the Debye−Scherer constant (k = 0.89), λ is the X-ray wavelength (λ = 0.15406 nm), β is the line broadening in radian obtained from the full width at half-maximum, and θ is the Bragg angle.[1] According to the Debye−Scherer equation, the average particle sizes of uncoated Fe_3O_4 and GFC are 30 and 35 nm, respectively.

The magnetization curves (Figure 1b) of Fe_3O_4 (curve (i)) and GFC nanocomposite (mass ratios of CS:Fe_3O_4:GO was 15:70:15 wt %) (curve (ii) show that both samples have superparamagnetic properties with the saturation magnetization (M_s) values of 70 and 42 emu g^{-1}, respectively). GO and CS are nonmagnetic. Thus, the magnetic behavior of the synthesized GFC materials came from the magnetite nanoparticle components. The lower M_s of GFC (42 emu g^{-1}) than that of Fe_3O_4 (M_s = 70 emu g^{-1}) can be attributed to the covered Fe_3O_4 nanoparticles by CS and GO, thereby reducing the saturation magnetization. However, the M_s of GFC is still very high (i.e., 42 emu/g), which is acceptable for magnetic separation using an external magnet in the recovery step. The hysteresis loop of the nitrogen (N_2) adsorption−desorption isotherm of the GFC nanocomposite exhibits type IV hysteresis loops by IUPAC, which is specific to mesoporous materials (pore width from 2 to 50 nm) (Figure 1c). The analyzed BET specific surface area of GFC nanocomposite is 134.36 m^2 g^{-1} with the BJH pore size distribution of 1.5−50 nm (Figure S2a) and the BJH adsorption/desorption average

https://doi.org/10.1021/acsomega.4c00486
ACS Omega 2024, 9, 17506−17517

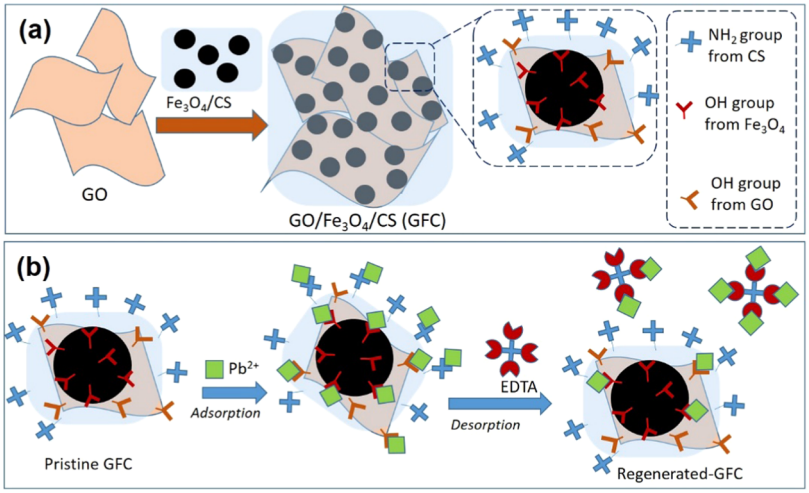

Figure 2. (a) Schematic diagram of GFC synthesis and its structure and specific function groups. (b) Strategy for using GFC as a smart and regenerable nanosorbent for Pb(II) adsorption.

pore width of 47.174/50.376 Å, which are in high agreement with the obtained hysteresis loop (Figure 1c). Raman spectrum (Figure 1d) of the Fe_3O_4 nanoparticle (line (i)) shows that the characteristic bands at 672 and 530 cm^{-1} are assigned to the A_{1g} and T_{2g} transitions of Fe_3O_4; meanwhile, the bands at 366, 709, and 1424 cm^{-1} can be attributed to the partial oxidation of the Fe_3O_4 surface to Fe_2O_3 maghemite and/or adsorbed CO_2 adsorption on the sample or the high laser power concentrated in a small area causing local heating, leading to phase transformation, oxidation, or decomposition of the sample.[42,43] The Raman spectra of GFC (line (ii)) and GO (line (iii)) show two main characteristic peaks of the carbon lattice structure known as a G-band at 1606 cm^{-1}, which corresponds to the E_{2g} vibration of sp^2-hybridized carbon atoms, and a D-band at 1346 cm^{-1}, which relates to the characteristic of crystal lattice defects during the oxidation process from graphite to GO, when the breaking of C=C double bonds occurs, leading to the formation of the sp^3-hybridized carbon.[43,44] In the Raman spectra of the GFC composite material, characteristic peaks of both Fe_3O_4 (a band at 672 cm^{-1}) and GO (D-band at 1346 cm^{-1} and G-band at 1606 cm^{-1}) are evident, confirming the successful synthesis of the desired composite material. TEM images of Fe_3O_4 nanoparticles (Figure 1e) show the presence of spherical Fe_3O_4 particles with a size of around 30−35 nm with high agglomeration. Meanwhile, the monodispersity of Fe_3O_4 nanoparticles loaded onto GO can be observed in the TEM image of GFC (Figure 1f). No free Fe_3O_4 can be found in the TEM image of GFC, which implies that GFC has been successfully fabricated with its structure, as described in Figure 2a. As shown in Figure S2b, pH_{PZC} of GFC is 4.4, which implies negative and positive GFC surface charges at pH >4.4 and pH <4.4, respectively.

The surface morphology of the synthesized materials can be observed in the SEM images (Figure 3). The pristine GO (Figure 3a−c) showed a sheet-like skeleton of carbon atoms with a flat surface and wrinkled edges. GO has a distinct layered structure, and graphene sheets have been identified through their folds. The wavy GO surface is randomly arranged, and their peeling is shown (Figure 3b,c). The SEM of Fe_3O_4 nanoparticles (Figure 3d−f) exhibits a spherical, relatively uniform crystal shape, and their surface morphology analysis shows the agglomeration of many ultrafine particles (approximately 10−15 nm) because of their magnetic nature.[30] This phenomenon can be explained by the specific surface energy, which is enormous at nanoparticle size. Thus, the particles tend to agglomerate to reduce the surface energy. The SEM of GFC (Figure 3g−i) shows that the GO sheet structures are densely covered with ferromagnetic particles, and these particles are coupled and densely distributed on the surface of the GO sheets due to the interactions between GO and CS. The SEM images show the desired result of material synthesis when promoting the role of components. GO can be relatively thin, and the ferromagnetic particles are spherical in shape and have a reasonably uniform size. CS helps the Fe_3O_4 particles to attach to the GO layer quite tightly. The GFC compositions were chemically investigated by a merged EDS mapping image (Figure 3j) and separated EDS mapping images, which indicated that C, Fe, N, and O were well distributed onto the GFC surface (Figure 3k−n, respectively). This finding is further proven by EDS results, showing the element contents of 77.1, 13.9, 8.4, 0.5, and 0.1% for Fe, O, C, Na, and N, respectively, in Figure 3j (inset). Therefore, the presence of GO, Fe_3O_4, and CS in the synthesized material is proven as desired.

Optimization Conditions for Pb(II) Up-Taking onto GFC Nanosorbent. The residue Pb(II) concentration was determined at different time intervals in the 0−120 min range, indicating that R_e rapidly increased to 51.32% in the first 5 min. It slowly increased to 57.60% after 50 min and remained almost constant for any contact time above 50 min (Figure 4a). These results suggested that the contact time of 50 min was considered the equilibrium time for further adsorption tests. To determine the best composition of CS: Fe_3O_4:GO for Pb(II) removal, different GFC compositions were prepared with mass ratios of CS:Fe_3O_4:GO as 15:60:25, 10:70:20, 10:80:10, and 15:70:15 wt %, and they were used as nanosorbent for Pb(II) removal with R_e vs contacting time (Figure 4b). For the GFC with ratios were 15:60:25, 10:70:20, and 10:80:10 wt %, the obtained R_e value was relatively low, around 20−30%; meanwhile, the R_e of GFC of 15:70:15 wt % reached 57.90%, which is a significant increase compared with those of the aforementioned samples. Therefore, the GFC composite had GO, Fe_3O_4, and CS in 15:70:15 wt %, the most

https://doi.org/10.1021/acsomega.4c00486
ACS Omega 2024, 9, 17506−17517

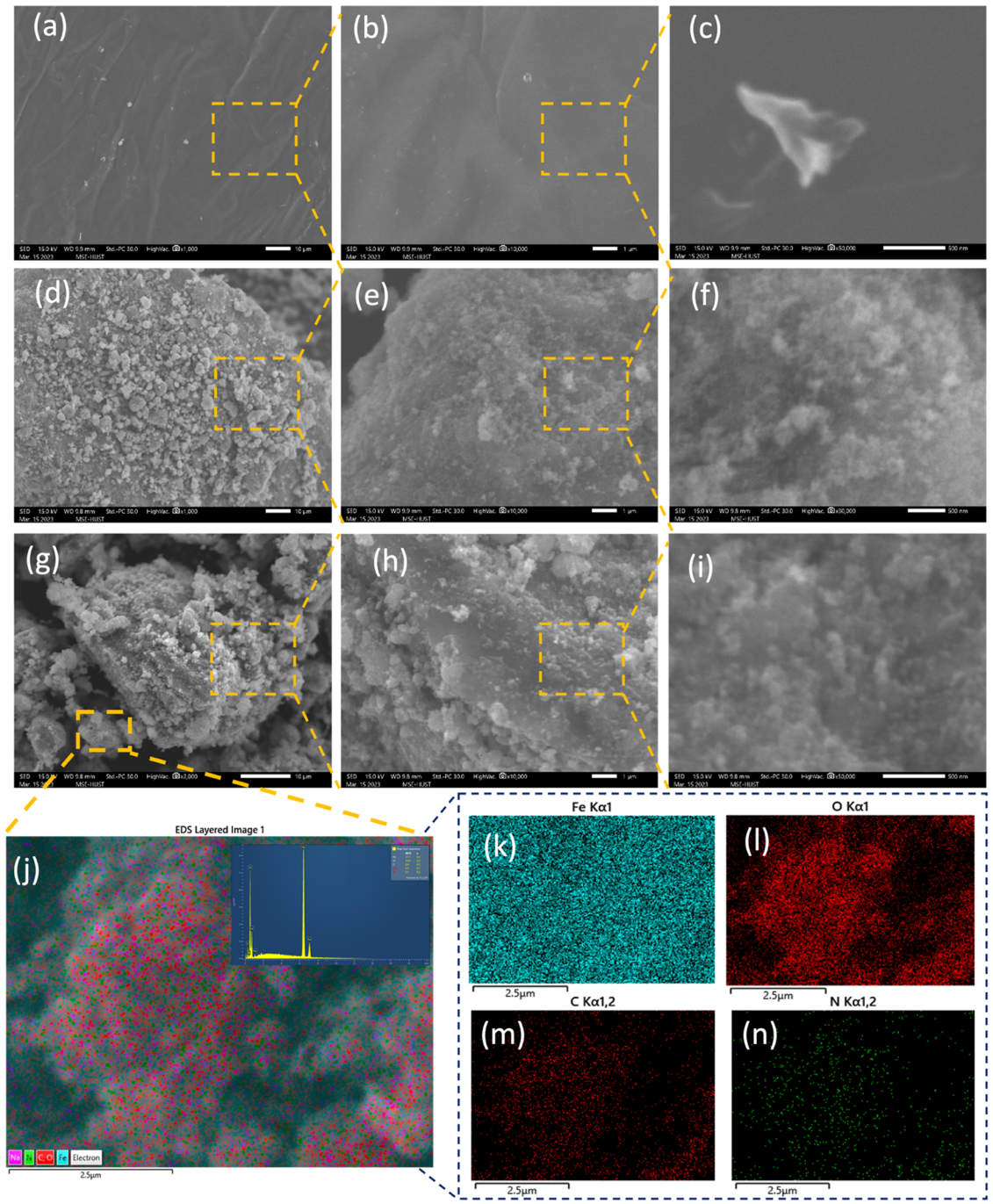

Figure 3. SEM images of (a−c) GO, (d−f) Fe_3O_4, and (g−i) GFC with different resolutions. (j) Merged EDS mapping images of N, C, O, and Fe for GFC nanocomposite. (k, l, m, n) EDS mapping of Fe, O, C, and N, respectively.

efficient adsorption among as-prepared composites. The tests of the single component including CS, GO, and Fe_3O_4 nanoparticles for Pb(II) adsorption and compared with GFC adsorbent at various concentrations of Pb(II) (from 10 to 70 mg L^{-1}) are shown in Figure SI4. It is clear that all single components have lower R_e values than the GFC composite at an applied concentration of Pb(II) (exception GO at 10 mg L^{-1} Pb(II)). Particularly, at a high concentration of Pb(II) (30−70 mg L^{-1}), the R_e values of CS, GO, and Fe_3O_4 nanoparticles decreased very fast, i.e., from R_e∼ 65.4/80% (at 10 mg L^{-1} Pb(II)) to R_e∼ 41.2/56.1% (at 30 mg L^{-1} Pb(II)) to R_e∼ 20.1/35.6% (at 70 mg L^{-1} Pb(II)); meanwhile, these R_e values were 70.2, 77.5, and 40%, respectively. These obtained results can be attributed to the synergistic effect of GO-Fe_3O_4 nanoparticles and CS, such as porous architecture (Figure 2a) or the presence of CS prevents any agglomeration of Fe_3O_4 and the presence of Fe_3O_4 nanoparticles prevents any reattachment of GO sheets. Figure 4b confirmed that the contacting time of 50 min is suitable for Pb(II) uptake onto the GFC nanosorbent. To compare, the adsorption of various heavy metal ions including Ni(II), Cd(II), Pb(II), and Cr(VI) (CrO_4^{2-}) onto GFC was tested, and the results in Figure S5 indicate that GFC selected to Pb(II) than that other ions.

The working pH influences the surface charge of the GFC and the electrostatic interactions between GFC and Pb(II). Therefore, the pH value directly affects the availability of

https://doi.org/10.1021/acsomega.4c00486
ACS Omega 2024, 9, 17506−17517

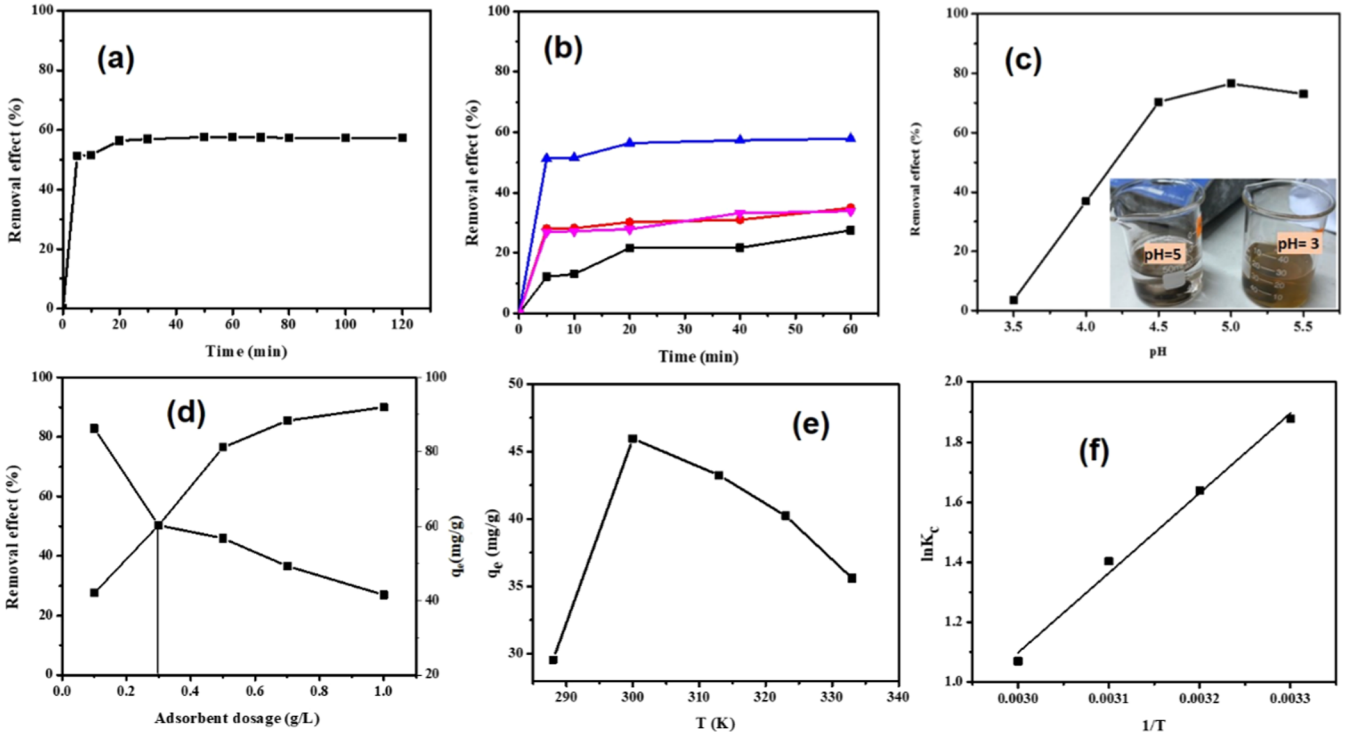

Figure 4. (a) Effects of contact time on Pb(II) removal efficiency (R_e), (b) effects of component ratio in the GFC composite on the R_e. (c) Effects of pH solution on the R_e (inset figure: digital photograph of the GFC nanosorbent in the Pb(II) solution at pH 3 and pH 5). (d) Effects of used GFC dosage on the R_e and equilibrium adsorption capacity (q_e) for Pb(II). (e) Effects of temperature on equilibrium adsorption capacity (q_e). (f) Van't Hoff plot for adsorption of Pb(II) on the GFC nanosorbent. Working conditions: adsorbent dosage of 0.5 g/L, Pb(II) concentration of 30 mg/L, pH of 5.0, and contacting bent time of 50 min.

Pb(II) ions in a solution and the metal binding sites of the adsorbent.[1] The pH_{PZC} of GFC is 4.4 (Figure SI2b); therefore, the positively charged Pb(II) ions can be easily uptaken onto the GFC surface at pH >4.4. However, when the working pH is <4.4, the competition between H^+ and Pb(II) increases and −OH and −COOH are protonated, thereby reducing the electrostatic interaction between GFC and Pb(II), as well as the adsorption capacity. As shown, R_e increased upon increasing the pH from 3.5 to 5.0 (Figure 4c), and the Pb(II) ion removal efficiency is best at pH 5, reaching 76.50%. As described by Yoshida,[45] at pH working <7, the Pb(II) ion exists in the form of free ions (Pb^{2+} and $PbOH^+$); meanwhile, at pH ≥7, the hydroxide and/or oxide species of Pb(II) are predominant ($Pb(OH)_2$, $[Pb(OH)_3]^-$, $[Pb_3(OH)_4]^{2+}$, $[Pb_6(OH)_8]^{4+}$, ...), and free Pb(II) is negligible, which leads a decrease in the adsorption capacity. When the pH is very low (i.e., <pH 3), Fe_3O_4 could be dissolved by

$$Fe_3O_4(s) + 8H^+(aq) \rightarrow 2Fe^{3+} + Fe^{2+} + 4H_2O \quad (5)$$

This reaction led to the release of Fe^{3+} ions, imparting the solution an orange-yellow color (Figure 4c, inset). Therefore, the working pH <3 is not suitable for working. In addition, the pH_{PZC} of the GFC composite was found to be approximately 4.4 (Figure S2b). Thus, the pH suitable for Pb(II) uptake onto the GFC adsorbent is pH 5. To make sure that the GFC is stable at pH working (i.e., pH 5) and there is no Fe_3O_4 which will release to iron ions in solution, a test with KCSN has been made (described in Section 6 of the Supporting Information), i.e., if there is iron ion in solution, the color of mixture with KSCN will be red and a specific peak at wavelength of 460 nm will be observed in UV−vis spectrum. As results show, no color and no absorption peak at 460 nm appeared in comparison with the control sample (mixture of 100 mL of 0.5 mM Fe^{3+} solution with 0.5 mL of 2 M KSCN) (Figure S6), implying that GFC is stable at working condition and no iron from GFC released to solution.

The effects of the amount of adsorbent on the removal were studied by changing the GFC concentrations from 0.1 to 1 g L^{-1}. The obtained data (Figure 4d) showed that the removal rate increased with the GFC dose, and when the dose increased from 0.1 to 1 g L^{-1}, the R_e for Pb(II) removal increased substantially while q_e decreased. R_e reached 90.0% Pb(II), and the corresponding q_e was 27.0 mg g^{-1}. This result demonstrated that the optimal removal rate was the intersection of q_e and R_e when the GFC dose was 0.3 g L^{-1}. Working temperature was evaluated (Figure 4e) from 15 to 60 °C. The results indicate that q_e is strongly dependent on temperature (i.e., q_e = 29.57, 45.95, 43.23, 40.23, and 35.60 mg g^{-1} were achieved at solution temperatures of 288, 300, 313, 323, and 333 K, respectively). The highest q_e value can be obtained at 300 K. Therefore, this temperature will be applied for further investigation. The initial Pb(II) ion concentration serves as a crucial driving force to overcome the mass transfer resistance of Pb(II) ions between the solid and aqueous phases. In many reactions, high concentrations of pollutants can promote a positive shift in the reaction equilibrium to a certain extent.[46] The effects of initial concentration were investigated by changing the concentrations of Pb(II) ions from 10 to 70 mg L^{-1}. The results are presented in Figure S4. At 10 mg L^{-1}, the lead ion concentration in the solution was low and the removal reaction did not work well. Thus, the removal rate was lower compared with other concentrations.

https://doi.org/10.1021/acsomega.4c00486
ACS Omega 2024, 9, 17506−17517

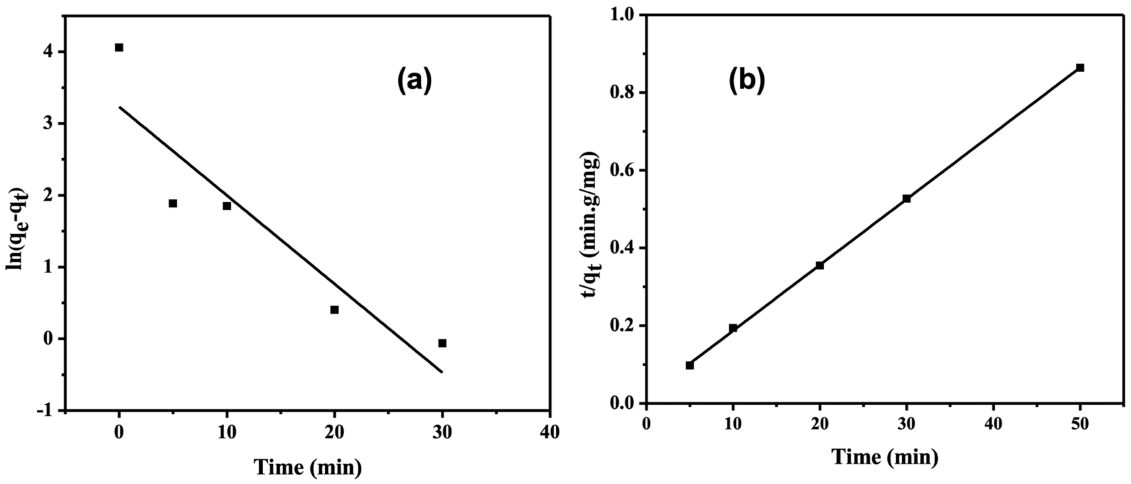

Figure 5. Pseudo (a) 1st-order kinetics, (b) 2nd-order kinetics for describing the adsorption of Pb(II) ions onto the GFC nanosorbent.

Table 1. Kinetic Parameters for the Adsorption of Pb(II) on GFC Nanosorbent

			pseudo-first-order model			pseudo-second-order model		
ion	C_o (mg L^{-1})	$q_{e,exp}$ (mg g^{-1})	$q_{e,cal}$ (mg g^{-1})	k_1 (min^{-1})	R^2	$q_{e,cal}$ (mg g^{-1})	k_2 (g mg^{-1} min^{-1})	R^2
Pb(II)	50	57.90	25.34	0.123	0.803	59.07	0.017	0.999

Apparently, the Pb(II) removal percentage increased with the initial concentration because a higher initial concentration promotes a positive shift in the reaction equilibrium, thereby resulting in a higher Pb(II) removal rate.[46] Furthermore, with the increase in the initial metal ion concentrations in water, the driving force for mass transfer and the adsorption capacity increased.[47,48] The maximum removal rate was observed when the initial concentration was 30 mg L^{-1}. The removal rate dropped as the initial concentration increased to 70 mg L^{-1}. For instance, increasing the initial Pb(II) concentration from 30 to 70 mg L^{-1} reduced the Pb(II) removal from 76.5 to 29.9%. This phenomenon might have occurred because the growth of the initial concentration increased the residual amount of Pb(II) in the aqueous solution. Thus, the removal efficiency declines. Furthermore, saturation of the adsorbent sites occurs at high Pb(II) concentrations. At higher Pb(II) concentrations, access to adsorption sites is somewhat limited, leading to reduced adsorption capacity. A maximum removal efficiency of 76.5% was achieved at 30 mg L^{-1}.

Adsorption Kinetic Model. The study of chemical kinetics can provide essential information on the adsorption rate and the factors that affect it. To assess dynamic characteristics, pseudo-first-order (1st-order) (eq 6) and pseudo-second-order (2nd-order) kinetic equations (eq 7) were applied to fit the experimental data linearly.

$$\ln(q_e - q_t) = \ln q_e - k_1 \cdot t \tag{6}$$

$$\frac{t}{q_t} = \frac{1}{k_2 q_e^2} + \frac{t}{q_e} \tag{7}$$

where q_t and q_e are the number of Pb(II) adsorbed (mg g^{-1}) at time t and at the equilibrium state, respectively; k_1 (min^{-1}) is the rate constant of the first-order kinetic model; and k_2 (g mg^{-1} min^{-1}) is the rate constant of the second-order kinetic model.

The obtained results (Figure 5 and Table 1) show that the second-order model has higher coefficient values (R^2 = 0.99) than the first-order model (R^2 = 0.803); moreover, the value of $q_{e(cal)}$ = 59.07 mg g^{-1} calculated from the second-order kinetic equation was close to $q_{e(exp.)}$ = 57.90 mg g^{-1} obtained from the experiment. This information indicates that the Pb(II) adsorption onto the GFC nanosorbent follows the second-order kinetic model, implying that the removal mechanism is a chemical process.

Adsorption Thermodynamics. To understand the kinetics of adsorption, the parameters of free energy ($\Delta G°$), enthalpy ($\Delta H°$), and entropy ($\Delta S°$) were determined by

$$\Delta G° = -RT \ln k_c \tag{8}$$

$$k_c = \frac{q_e}{C_e} \tag{9}$$

$$\ln k_c = -\frac{\Delta H°}{RT} + \frac{\Delta S°}{R} \tag{10}$$

where k_c is the equilibrium constant, (q_e/C_e) is the distribution coefficient, T is the temperature in Kelvin, and R is the universal gas constant (8.314 J mol^{-1} K^{-1}).

The thermodynamic parameters for Pb(II) adsorption onto GFC were evaluated from eqs 8−10 at four different temperatures. The results have been plotted as a Van't Hoff plot (Figure 2f) and the data in Table 2. The value of $\Delta G°$ is negative at all temperatures, and it changed from −4.684 to −2.962 kJ mol^{-1} when the temperature increased from 300 to 333 K, which indicates that the adsorption of Pb(II) on GFC was a spontaneous process. The value of $\Delta G°$ became more positive with the increase in temperature, implying that a

Table 2. Thermodynamic Parameters

temperature (K)	$\ln k_c$	$\Delta G°$ (kJ mol^{-1})	$\Delta H°$ (kJ mol^{-1})	$\Delta S°$ (J mol^{-1} K^{-1})
300	1.878	−4.684	−22.119	−57.223
313	1.640	−4.268		
323	1.404	−3.770		
333	1.070	−2.962		

https://doi.org/10.1021/acsomega.4c00486
ACS Omega 2024, 9, 17506−17517

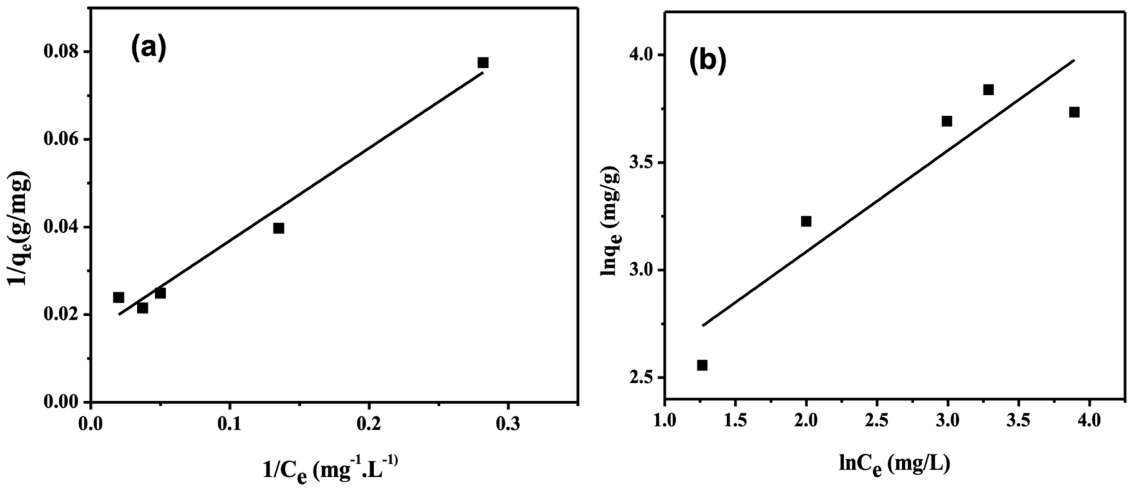

Figure 6. (a) Langmuir and (b) Freundlich's isotherms for Pb(II) adsorption on GFC nanosorbent.

higher temperature was less favorable for the adsorption of Pb(II) on GFC. The negative value $\Delta H^\circ = -22.119$ kJ mol^{-1} confirmed the exothermic nature of adsorption, which was also supported by the decline in the Pb(II) adsorption removal ratios when the temperature increased. Furthermore, the negative value of $\Delta S^\circ = 57.223$ J mol^{-1} K^{-1} reflected a decrease in the adsorbed species' freedom. In addition, the attractive forces between the surface and metal ions were weakened, leading to reduced adsorption.[49] However, the Pb(II) adsorption mechanism of GFC materials was chemisorption, an exothermic process that occurs slowly at low temperatures, so the adsorption capacity at 15 °C (288 K) was the lowest.

Adsorption Isotherms. The adsorption isotherm shows how the adsorbed molecules distribute between the liquid and solid phases when the adsorption equilibrium has been established. The adsorption isotherm studies were performed by following Langmuir and Freundlich models. The Langmuir model (eq 11) assumes that adsorption occurs on a homogeneous surface by monolayer coverage, and no subsequent interaction was observed between adsorbed species. The Freundlich model (eq 12) is an empirical model based on multiplayer adsorption on heterogeneous surfaces.

$$\frac{1}{q_e} = \frac{1}{q_{max}} + \frac{1}{C_e \cdot k_L \cdot q_{max}} \tag{11}$$

$$\ln q_e = \ln k_F + \frac{1}{n} \ln C_e \tag{12}$$

where C_e (mg L^{-1}) is the equilibrium concentration; q_e (mg g^{-1}) is the equilibrium adsorption capacity; q_{max} (mg g^{-1}) represents the maximum adsorption capacity; k_L and k_F are the Langmuir and Freundlich adsorption constant, respectively; and n is the Freundlich exponential coefficient.

The Langmuir and Freundlich isotherm models fitted with experimental data were presented in Figure 6 and Table 3. The showed that the R^2 value of the Langmuir isotherm (R^2 = 0.965) is higher than that of the Freundlich isotherm (R^2 = 0.820) and closer to the q_{max} value to that experimental one. From this, it can be concluded that the Langmuir model fits better than the Freundlich model for adsorption of Pb(II) on GFC nanosorbent, indicating that Pb(II) adsorption occurs on a monolayer surface of GFC nanosorbent with active sites of uniform energies.[50] The empirical parameter $1/n$ was 0.47 (within 0.1−1.0), which shows that the adsorption was easy.[51]

Table 3. Adsorption Isotherm Parameters

Langmuir			Freundlich		
q_{max} (mg g^{-1})	k_L (L mg^{-1})	R^2	k_F (mg g^{-1})	n	R^2
63.45	0.075	0.965	8.53	2.12	0.820

Regeneration Ability of GFC Nanosorbent. As shown by the obtained results, the GFC nanosorbent exhibited a good adsorption capability (q_{max}). Therefore, the regeneration and stability of adsorbents are crucial for their practical application. Reusability is a critical aspect of assessing the practicability of any newly developed adsorbent.[52] In the present study, 0.05 M Na_2EDTA was selected as a desorption reagent for the adsorbed Pb(II) ion. The reusability of GFC was examined under certain conditions including Pb(II) concentration of 30 mg L^{-1}, pH 5.0 at RT with an adsorbent dosage of 0.5 g L^{-1}, and contacting time of 50 min. Adsorption−desorption experiments were repeated over four cycles and conducted as follows: the material after Pb(II) adsorption was soaked in a 0.05 M Na_2EDTA solution for 2 h. Subsequently, the material was collected using an external magnet from the solution (Figure 7a,b) and dried in an oven at 45 °C for 24 h. As shown in Figure 7c, the removal efficiency of Pb(II) using regenerated GFC decreased as the number of recycles increased. The result depicts that the adsorption percentage of Pb(II) by GFC composite material decreased from 76.5 to 64.0% after four consecutive cycles (approximately 12% reduction after four cycles). This phenomenon may be due to the incomplete Pb(II) desorption. As a conclusion, the synthesized composite could act as a renewable and stable candidate adsorbent for practical application. Based on adsorption/desorption and regeneration results, a working mechanism is proposed in Figure 2b, herein, Pb(II) ions were uptaken onto the GFC nanosorbent via various interaction focuses, including (i) the electrostatic interaction between the positive charge of Pb(II) ions with a negative charge of carboxylic groups (−COO^-) and/or hydroxyl groups (−OH^-) of GO sheets on the GFC surface, (ii) coordination bonding between unpaired electron pairs on amino groups (−NH_2) of CS or conjugated π-electrons with vacant d-atomic orbital of Pb(II) ions.

https://doi.org/10.1021/acsomega.4c00486
ACS Omega 2024, 9, 17506−17517

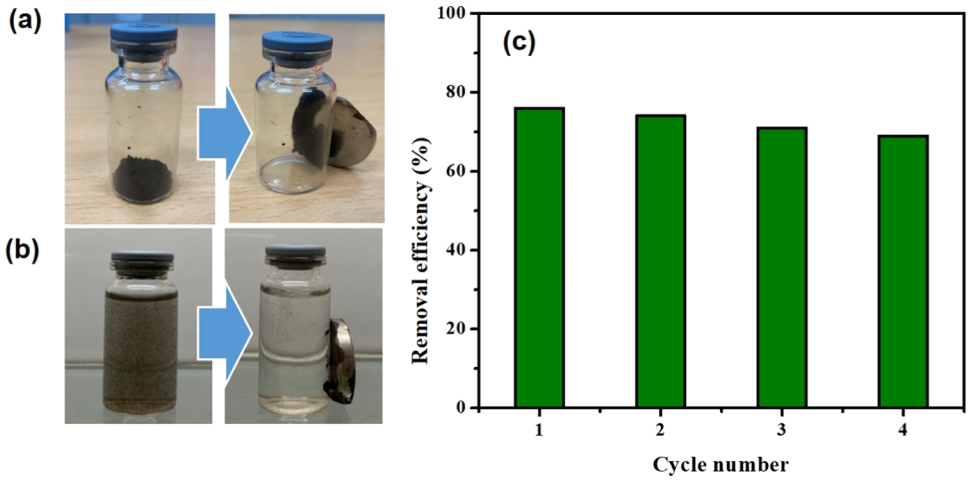

Figure 7. (a, b) Digital photographs of (a) GFC nanosorbent as a powder with substantial magnetic property, (b) GCE nanosorbent in the working solution and removed by magnetic separation, and (c) R_e vs recycle numbers of GFC nanosorbent for Pb(II) removal.

Table 4. Comparison of Adsorption Capacities (q_{max}) of Various Adsorbents for Pb(II) Removal

adsorbents	optimized conditions	q_{max} (mg/g)	recycle conditions	refs
CS/Fe_3O_4	temperature: *RT*, contacting time: 2 h, pH 6, dosage of adsorbent 0.1 g L^{-1} and Pb(II) concentration range: 50−80 mg L^{-1}	63.33	N/A*	1
sepiolite modified sepiolite by inorganic liquid (as@sep)	*RT*, pH 5.0, contact time:180 min, and initial Pb(II) concentration: 50 mg L^{-1}	31.98	N/A*	3
smart graphene oxide nanocomposites (MGO@PNB)	pH 5.0, T = 25 °C, contact time: 20 min	11.76	N/A*	6
GO/CS hydrogel	temperature: *RT*, contacting time: 4 h, pH 4.9, dosage of adsorbent 0.125 g L^{-1} and Pb(II) concentration range: N/A*	90	N/A*	27
Fe_3O_4/GO	temperature: 30 °C, contacting time: 1 h, pH 5, dosage of adsorbent 0.8 g L^{-1} and Pb(II) concentration range: N/A*	31.6	desorption reagent: HCl, desorption time: 48 h, temperature: *RT* and recycle numbers: 5	28
GO−CS-poly(acrylic acid)	temperature: *RT*, contacting time: 24 h, pH 5, dosage of adsorbent 37.5 g L^{-1} and Pb(II) concentration range: 50−250 mg L^{-1}	138.89	desorption reagent: 0.1 M HCl, desorption time: 24 h, temperature: *RT* and recycle numbers: 3	29
graphene oxides (GOs)	temperature: 25 °C, contacting time: 10 min, pH 5, dosage of adsorbent 0.5 g L^{-1} and Pb(II) concentration range: 5−60 mg L^{-1}	120	N/A*	53
Fe_3O_4/CS/GO	temperature: *RT*, contacting time: 40 min, pH 4−7, adsorbent dosage 0.3 g L^{-1}. Pb(II) concentration range: N/A*	76.94	desorption reagent: CH_3COOH (concentration: N/A*), desorption time: N/A* temperature: N/A* and recycle numbers: 6	54
$GO/Fe_3O_4/CS$	temperature: *RT*, contacting time: 50 min, pH 5, dosage of adsorbent 0.5 g L^{-1} and Pb(II) concentration range: 10−70 mg L^{-1}	63.45	desorption reagent: 0.05 M Na_2EDTA, desorption time: 2 h, temperature: *RT*, and recycle numbers: >4	this study

N/A*: information(s) was not given.

Table 4 lists the assessment of the adsorption capacities for the synthesized GFC composite material and other adsorbents in the literature for the removal of Pb(II). q_{max} of the synthesized GFC nanosorbent for Pb(II) adsorption is 63.45 mg g^{-1}, which can be comparable and even higher than those of other magnetite (Fe_3O_4)-based adsorbents for Pb(II). Still, the adsorption capacity of the GFC nanosorbent was slightly lower than that of the non-Fe_3O_4-based adsorbent (90−138.89 mg g^{-1}). This result could be due to structural morphology. The surface area and functional groups of the adsorbent affected the adsorption capacity of the materials. However, owing to good reusability, simple synthesis, and thermal stability, our composite beads will have an economic advantage over their counterpart. Hence, they can be used as a promising adsorbent to remove Pb(II) ions.

CONCLUSIONS

As a nanosorbent, the GFC composite has shown a high potential and a high adsorption capacity for removing Pb(II) ions from aqueous solutions. The characterization results verified the successful synthesis of the adsorbent with remarkable magnetic properties. The GFC nanosorbent briefly exhibited superior adsorption capacity for Pb(II) uptake from water samples. As estimated, with an initial concentration of 30 mg L^{-1}, 90% of Pb(II) ions were removed at an equilibrium time of 50 min, a pH of 5, and an adsorbent dosage of 1 g L^{-1} at 27 °C. The maximum amount of adsorbed Pb(II) was nearly 63.45 mg g^{-1}. The thermodynamic study also reveals that the adsorption efficiency is more favorable at lower temperatures, preferably at room temperature (27 °C). Kinetic studies indicated that the adsorption of Pb(II) onto the GFC followed the second-order kinetic model, indicating that the Pb(II) ions are adsorbed onto the GFC composite material through a chemisorption process. Additionally, compared with the

https://doi.org/10.1021/acsomega.4c00486
ACS Omega 2024, 9, 17506−17517

Freundlich isotherm model, the Langmuir model best fits the adsorption process. The negative value ΔH° (22.119 kJ mol^{-1}) confirmed the exothermic nature of adsorption. Finally, the removal efficiency (R_e) was reduced by only approximately 12% after four adsorption−desorption cycles. This finding suggested high regeneration and stability, manifesting its great potential in practical applications.

■ ASSOCIATED CONTENT

Supporting Information

The Supporting Information is available free of charge at https://pubs.acs.org/doi/10.1021/acsomega.4c00486.

Additional experimental details, materials, and methods, including photographs of the experimental setup for the synthesis of GO; BJH pore size distribution of GFC nanocomposite; the initial pH vs tested pH curve for pH_{PZC} investigation; UV−vis spectra and calibration curve for Pb(II) concentration determination; adsorption of Pb(II) onto various adsorbents at various initial concentrations of Pb(II); the adsorption of various metal ions onto GFC adsorbent; UV−vis spectra of mixtures of the KSCN solution with Fe^{3+} solution and supernatant solutions after adsorptions using GFC and Fe_3O_4 nanoparticle as adsorbents (PDF)

■ AUTHOR INFORMATION

Corresponding Author

Hoang Vinh Tran − *School of Chemistry and Life Sciences, Hanoi University of Science and Technology, Hanoi 10000, Vietnam*; orcid.org/0000-0003-1777-5526; Email: hoang.tranvinh@hust.edu.vn

Authors

Linh Quang Vo − *School of Chemistry and Life Sciences, Hanoi University of Science and Technology, Hanoi 10000, Vietnam*

Anh-Tuan Vu − *School of Chemistry and Life Sciences, Hanoi University of Science and Technology, Hanoi 10000, Vietnam*

Thu Dieu Le − *School of Chemistry and Life Sciences, Hanoi University of Science and Technology, Hanoi 10000, Vietnam*

Chinh Dang Huynh − *School of Chemistry and Life Sciences, Hanoi University of Science and Technology, Hanoi 10000, Vietnam*

Complete contact information is available at: https://pubs.acs.org/10.1021/acsomega.4c00486

Author Contributions

L.Q.V. (first author) wrote the original draft and was responsible for visualization, data curation, formal analysis, investigation, and software. A.-T.V. (second author) edited the manuscript and performed the formal analysis and data curation. T.D.L. (third author) was responsible for visualization, formal analysis, investigation, and data curation. C.D.H. (fourth author) performed the formal analysis, edited the manuscript, and curated the data. H.V.T. (corresponding author) was responsible for the conceptualization, methodology, supervision, reviewing and editing, and validation.

Notes

The authors declare no competing financial interest.

■ ACKNOWLEDGMENTS

This research is funded by the Vietnam Ministry of Education and Training (MOET) under grant number CT2022.04.BKA.01.

■ REFERENCES

(1) Tran, V. H.; Tran, D. T.; Nguyen, N. T. Preparation of chitosan/magnetite composite beads and their application for removal of Pb (II) and Ni (II) from aqueous solution. *Mater. Sci. Eng., C* **2010**, *30*, 304−310.

(2) Samuel, S. M.; Shah, S. S.; Bhattacharya, J.; Subramaniam, K.; Singh, D. P. N. Adsorption of Pb (II) from aqueous solution using a magnetic chitosan/graphene oxide composite and its toxicity studies. *Int. J. Biol. Macromol.* **2018**, *115*, 1142−1150.

(3) Gu, Y.; Feng, H.; Wang, B.; Qiu, J.; Meng, X.; Zhang, L.; Zhang, B.; Chen, N.; Tan, L. Adsorption of Pb2+ by inorganic liquid-treated sepiolite: Adsorption process optimization and mechanism analysis via response surface methodology. *Microporous Mesoporous Mater.* **2024**, *363*, No. 112821.

(4) Mohammadi, A.; Jafarpour, E.; Mirzaei, K.; Shojaei, A.; Jafarpour, P.; Eyni, B. M.; Mirzaei, S.; Molavi, H. Novel ZIF-8/CNC Nanohybrid with an Interconnected Structure: Toward a Sustainable Adsorbent for Efficient Removal of Cd(II) Ions. *ACS Appl. Mater. Interfaces* **2024**, *16*, 3862−3875.

(5) Li, Y.; Shuai, X.; Zhang, M.; Ma, F.; Chen, J.; Qiao, J.; Chen, R.; Du, L. Preparation of ethylenediamine-modified pectin/alginate/Fe3O4 microsphere and its efficient Pb2+ adsorption properties. *Int. J. Biol. Macromol.* **2022**, *223*, 173−183.

(6) Pan, L.; Zhai, G.; Yang, X.; Yu, H.; Cheng, C. Thermosensitive Microgels-Decorated Magnetic Graphene Oxides for Specific Recognition and Adsorption of Pb(II) from Aqueous Solution. *ACS Omega* **2022**, *4*, 3933−3945.

(7) Ren, Y.; Abbood, H. A.; He, F.; Peng, H.; Huang, K. Magnetic EDTA-modified chitosan/SiO2/Fe3O4 adsorbent: preparation, characterization, and application in heavy metal adsorption. *Chem. Eng. J.* **2013**, *226*, 300−311.

(8) Heidari, A.; Younesi, H.; Mehraban, Z.; Heikkinen, H. Selective adsorption of Pb (II), Cd (II), and Ni (II) ions from aqueous solution using chitosan−MAA nanoparticles. *Int. J. Biol. Macromol.* **2013**, *61*, 251−263.

(9) Duan, S.; Tang, R.; Xue, Z.; Zhang, X.; Zhao, Y.; Zhang, W.; Zhang, J.; Wang, B.; Zeng, S.; Sun, D. Effective removal of Pb (II) using magnetic Co0. 6Fe2. 4O4 micro-particles as the adsorbent: synthesis and study on the kinetic and thermodynamic behaviors for its adsorption. *Colloids Surf., A* **2015**, *469*, 211−223.

(10) Yan, Y.; Li, Q.; Sun, X.; Ren, Z.; He, F.; Wang, Y.; Wang, L. Recycling flue gas desulphurization (FGD) gypsum for removal of Pb (II) and Cd (II) from wastewater. *J. Colloid Interface Sci.* **2015**, *457*, 86−95.

(11) Wang, W.; Zhao, Y.; Yi, H.; Chen, T.; Kang, S.; Zhang, T.; Rao, F.; Song, S. Pb (II) removal from water using porous hydrogel of chitosan-2D montmorillonite. *Int. J. Biol. Macromol.* **2019**, *128*, 85−93.

(12) Denizli, A.; Senel, S.; Alsancak, G.; Tüzmen, N.; Say, R. Mercury removal from synthetic solutions using poly (2-hydroxyethylmethacrylate) gel beads modified with poly (ethyleneimine). *React. Funct. Polym.* **2003**, *55*, 121−130.

(13) Ngah, S. W. W.; Kamari, A.; Koay, J. Y. Equilibrium and kinetics studies of adsorption of copper (II) on chitosan and chitosan/PVA beads. *Int. J. Biol. Macromol.* **2004**, *34*, 155−161.

(14) Varma, J. A.; Deshpande, V. S.; Kennedy, F. J. Metal complexation by chitosan and its derivatives: a review. *Carbohydr. Polym.* **2004**, *55*, 77−93.

(15) Atia, A. A.; Donia, M. A.; Shahin, E. A. Studies on the uptake behavior of a magnetic Co3O4-containing resin for Ni (II), Cu (II) and Hg (II) from their aqueous solutions. *Sep. Purif. Technol.* **2005**, *46*, 208−213.

(16) Justi, C. K.; Fávere, T. V.; Laranjeira, C. M. M.; Neves, A.; Peralta, A. R. Kinetics and equilibrium adsorption of Cu (II), Cd (II), and Ni (II) ions by chitosan functionalized with 2 [-bis-(pyridylmethyl) aminomethyl]-4-methyl-6-formylphenol. *J. Colloid Interface Sci.* **2005**, *291*, 369−374.
(17) Chang, Y.-C.; Chang, S.-W.; Chen, D.-H. Magnetic chitosan nanoparticles: Studies on chitosan binding and adsorption of Co (II) ions. *React. Funct. Polym.* **2006**, *66*, 335−341.
(18) Xuan, S.; Hao, L.; Jiang, W.; Gong, X.; Hu, Y.; Chen, Z. Preparation of water-soluble magnetite nanocrystals through hydrothermal approach. *J. Magn. Magn. Mater.* **2007**, *308*, 210−213.
(19) Namdeo, M.; Bajpai, S. K. Chitosan−magnetite nanocomposites (CMNs) as magnetic carrier particles for removal of Fe (III) from aqueous solutions. *Colloids Surf., A* **2008**, *320*, 161−168.
(20) An, T. N.; Thien, T. D.; Dong, T. N.; Dung, L. P. Water-soluble N-carboxymethylchitosan derivatives: Preparation, characteristics and its application. *Carbohydr. Polym.* **2009**, *75*, 489−497.
(21) Zhou, Y.-T.; Nie, H.-L.; Branford-White, C.; He, Z.-Y.; Zhu, L.-M. Removal of Cu2+ from aqueous solution by chitosan-coated magnetic nanoparticles modified with α-ketoglutaric acid. *J. Colloid Interface Sci.* **2009**, *330*, 29−37.
(22) Zhang, Y.; Li, Y.; Li, X.; Yang, L.; Bai, X.; Ye, Z.; Zhou, L.; Wang, L. Selective removal for Pb2+ in aqueous environment by using novel macroreticular PVA beads. *J. Hazard. Mater.* **2010**, *181*, 898−907.
(23) Hajdu, I.; Bodnár, M.; Csikós, Z.; Wei, S.; Daróczi, L.; Kovács, B.; Győri, Z.; Tamás, J.; Borbély, J. Combined nano-membrane technology for removal of lead ions. *J. Membr. Sci.* **2012**, *409*, 44−53.
(24) Zhang, F.; Wang, B.; He, S.; Man, R. Preparation of graphene-oxide/polyamidoamine dendrimers and their adsorption properties toward some heavy metal ions. *J. Chem. Eng. Data* **2014**, *59*, 1719−1726.
(25) Wang, Y.; Li, L. L.; Luo, C.; Wang, X.; Duan, H. Removal of Pb2+ from water environment using a novel magnetic chitosan/graphene oxide imprinted Pb2+. *Int. J. Biol. Macromol.* **2016**, *86*, 505−511.
(26) Xu, J.; Cao, Z.; Zhang, Y.; Yuan, Z.; Lou, Z.; Xu, X.; Wang, X. A review of functionalized carbon nanotubes and graphene for heavy metal adsorption from water: Preparation, application, and mechanism. *Chemosphere* **2018**, *195*, 351−364.
(27) Chen, Y.; Chen, L.; Bai, H.; Li, L. Graphene oxide−chitosan composite hydrogels as broad-spectrum adsorbents for water purification. *J. Mater. Chem. A* **2013**, *1*, 1992−2001.
(28) Fan, L.; Luo, C.; Sun, M.; Li, X.; Qiu, H. Highly selective adsorption of lead ions by water-dispersible magnetic chitosan/graphene oxide composites. *Colloids Surf., B* **2013**, *103*, 523−529.
(29) Medina, P. R.; Nadres, T. E.; Ballesteros, F. C.; Rodrigues, F. D. Incorporation of graphene oxide into a chitosan−poly (acrylic acid) porous polymer nanocomposite for enhanced lead adsorption. *Environ. Sci.: Nano* **2016**, *3*, 638−646.
(30) Zhao, D.; Gao, X.; Wu, C.; Xie, R.; Feng, S.; Chen, C. Facile preparation of amino functionalized graphene oxide decorated with Fe3O4 nanoparticles for the adsorption of Cr (VI). *Appl. Surf. Sci.* **2016**, *384*, 1−9.
(31) Tran, V. H.; Huynh, D. C.; Tran, D. L. Chapter 4 - Recoverable and Regenerable Magnetite-Based Nanocomposite Adsorbents for Heavy Metal Removal in Contaminated Water. In *Green Sustainable Process for Chemical and Environmental Engineering and Science: Applications of Advanced Nanostructured Materials in Wastewater Remediation*; Inamuddin, T. A.; Mazumder, M. A. J., Eds.; Elsevier, 2023; pp 113−154.
(32) Cestari, R. A.; Vieira, F. S. E.; de Oliveira, A. I.; Bruns, E. R. The removal of Cu (II) and Co (II) from aqueous solutions using cross-linked chitosan—evaluation by the factorial design methodology. *J. Hazard. Mater.* **2007**, *143*, 8−16.
(33) Jiang, W.; Wang, W.; Pan, B.; Zhang, Q.; Zhang, W.; Lv, L. Facile fabrication of magnetic chitosan beads of fast kinetics and high capacity for copper removal. *ACS Appl. Mater. Interfaces* **2014**, *6*, 3421−3426.
(34) Fan, C.; Li, K.; He, Y.; Wang, Y.; Qian, X.; Jia, J. Evaluation of magnetic chitosan beads for adsorption of heavy metal ions. *Sci. Total Environ.* **2018**, *627*, 1396−1403.
(35) Saad, A. H. A.; Azzam, M. A.; El-Wakeel, T. S.; Mostafa, B. B.; Abd El-latif, B. M. Removal of toxic metal ions from wastewater using ZnO@ Chitosan core-shell nanocomposite. *Environ. Nanotechnol., Monit. Manage.* **2018**, *9*, 67−75.
(36) Sun, M.; Cheng, G.; Ge, X.; Chen, M.; Wang, C.; Lou, L.; Xu, X. Aqueous Hg (II) immobilization by chitosan stabilized magnetic iron sulfide nanoparticles. *Sci. Total Environ.* **2018**, *621*, 1074−1083.
(37) Annadurai, G.; Ling, Y. L.; Lee, F. J. Adsorption of reactive dye from an aqueous solution by chitosan: isotherm, kinetic and thermodynamic analysis. *J. Hazard. Mater.* **2008**, *152*, 337−346.
(38) Bhatt, R.; Sreedhar, B.; Padmaja, P. Adsorption of chromium from aqueous solutions using crosslinked chitosan−diethylenetriaminepentaacetic acid. *Int. J. Biol. Macromol.* **2015**, *74*, 458−466.
(39) Bertoni, A. F.; González, C. J.; García, S. I.; Sala, F. L.; Bellú, E. S. Application of chitosan in removal of molybdate ions from contaminated water and groundwater. *Carbohydr. Polym.* **2018**, *180*, 55−62.
(40) Ju, H.-M.; Choi, S.-H.; Huh, S. H. X-ray diffraction patterns of thermally-reduced graphenes. *J. Korean Phys. Soc.* **2010**, *57*, 1649.
(41) Chowdhuri, R. A.; Tripathy, S.; Chandra, S.; Roy, S.; Sahu, K. S. A ZnO decorated chitosan−graphene oxide nanocomposite shows significantly enhanced antimicrobial activity with ROS generation. *RSC Adv.* **2015**, *5*, 49420−49428.
(42) Qi, H.; Ye, J.; Tao, N.; Wen, M.; Chen, Q. Synthesis of octahedral magnetite microcrystals with high crystallinity and low coercive field. *J. Cryst. Growth* **2009**, *311*, 394−398.
(43) Hatel, R.; Majdoub, E. S.; Bakour, A.; Khenfouch, M.; Baitoul, M. Graphene oxide/Fe3O4 nanorods composite: structural and Raman investigation. *J. Phys.: Conf. Ser.* **2018**, *1081*, No. 012006.
(44) Le, T. T. N.; Tran, V. H.; Huynh, D. C.; Nguyen, D. C.; Phi, V. T. Thermal Exfoliated Graphite/Chitosan Modified Glassy Carbon Electrode for Cu(II) Ion Sensing. *Curr. Anal. Chem.* **2022**, *18*, 790−797.
(45) Yoshida, T.; Yamaguchi, T.; Iida, Y.; Nakayama, S. XPS study of Pb (II) adsorption on γ-Al2O3 surface at high pH conditions. *J. Nucl. Sci. Technol.* **2003**, *40*, 672−678.
(46) Li, R.; Li, Q.; Sun, X.; Li, J.; Shen, J.; Han, W.; Wang, L. Efficient and rapid removal of EDTA-chelated Pb (II) by the Fe (III)/flue gas desulfurization gypsum (FGDG) system. *J. Colloid Interface Sci.* **2019**, *542*, 379−386.
(47) Wasewar, K. L. Adsorption of metals onto tea factory waste: a review. *Int. J. Res.* **2010**, *3*, 303−322.
(48) Javadian, H.; Vahedian, P.; Toosi, M. Adsorption characteristics of Ni (II) from aqueous solution and industrial wastewater onto Polyaniline/HMS nanocomposite powder. *Appl. Surf. Sci.* **2013**, *284*, 13−22.
(49) Jnr, M. H.; Spiff, A. I. Effects of temperature on the sorption of Pb2+ and Cd2+ from aqueous solution by Caladium bicolor (Wild Cocoyam) biomass. *Electron. J. Biotechnol.* **2005**, *8*, 43−50.
(50) Homayonfard, A.; Miralinaghi, M.; Shirazi, H. S. M. R.; Moniri, E. Efficient removal of cadmium (II) ions from aqueous solution by CoFe2O4/chitosan and NiFe2O4/chitosan composites as adsorbents. *Water Sci. Technol.* **2018**, *78*, 2297−2307.
(51) Jiang, Q. M.; Wang, P. Q.; Jin, Y. X.; Chen, I. Z. Removal of Pb (II) from aqueous solution using modified and unmodified kaolinite clay. *J. Hazard. Mater.* **2009**, *170*, 332−339.
(52) Fang, Y.; Huang, Q.; Liu, P.; Shi, J.; Xu, G. Easy-separative MoS2-glue sponges with high-efficient dye adsorption and excellent reusability for convenient water treatment. *Colloids Surf., A* **2018**, *540*, 112−122.
(53) Raghubanshi, H.; Ngobeni, S. M.; Osikoya, A. O.; Shooto, N. D.; Dikio, C. W.; Naidoo, E. B.; Dikio, E. D.; Pandey, R. K.; Prakash, R. Synthesis of graphene oxide and its application for the adsorption of Pb2+ from aqueous solution. *J. Ind. Eng. Chem.* **2017**, *47*, 169−178.

https://doi.org/10.1021/acsomega.4c00486
ACS Omega 2024, 9, 17506−17517

(54) Liu, X.; Hu, Q.; Fang, Z.; Zhang, X.; Zhang, B. Magnetic chitosan nanocomposites: a useful recyclable tool for heavy metal ion removal. *Langmuir* **2009**, *25*, 3−8.

https://doi.org/10.1021/acsomega.4c00486
ACS Omega 2024, 9, 17506−17517